

Spontaneous Radiofrequency Emission from Electron Spins within *Drosophila*: a preliminary report on a novel biological signal.

Alexandros Gaitanidis^a, Antonello Sotgiu^b and Luca Turin^{1a}

^aNeuroscience Division, BSRC Alexander Fleming, 16672 Vari, Greece

^bApplied Physics, University of L'Aquila, 67100 L'Aquila, Italy

Abstract: Using simple radiofrequency (RF) instrumentation, we detect spontaneous RF emission from *Drosophila* immersed in a magnetic field within a waveguide or a shielded RF resonator. Remarkably, the RF emissions are abolished by chloroform anesthesia, suggesting that they come from the nervous system. RF frequency and magnetic field dependence are consistent with RF emission being related to electron Zeeman energy. Since the RF emission occurs without external energy input, its energy must come from cell metabolism. We propose that RF emissions are due to *in vivo* spin-polarised cellular electron currents. We suggest that spin-polarised currents relax radiatively to equilibrium at the Larmor frequency and are detected under our experimental conditions (resonator cavity and lock-in detection). We publish this preliminary report to invite scrutiny of our methods and results, elicit theorists' interest in this novel phenomenon, and encourage replication in this and other preparations.

Introduction. The work of Naaman and others (Gutierrez, Díaz, Naaman, & Cuniberti, 2012; Ron Naaman, Paltiel, & Waldeck, 2018; Naaman & Waldeck, 2012; Varade et al., 2018; Zwang, Hürlimann, Hill, & Barton, 2016) has shown that electrons traversing chiral phases such as proteins and DNA become spin-polarised in the direction of travel. In aerobic organisms, large electron currents (100 A in a human at rest (Rees, 1983), 1 μ A in a single 1-mg fruit fly (Hunter, 1964), both under approximately 1.4V) reduce dioxygen to water. These currents flow through chiral proteins, and their spin polarisation by the same mechanism is therefore likely. Such spin-polarised electron currents may at some point exit a chiral phase but will generally not be oriented in a specific spatial direction, since the cellular circuits in which they flow are randomly oriented. A snapshot of electrons exiting a chiral phase will, therefore, even if spin-polarized, not differ from a population of spins at thermal equilibrium. In a magnetic field, however, some anisotropy may arise from magnetic reorientation of the medium carrying the electron currents (Iwasaka, Miyakoshi, & Ueno, 2003; Kotani, Iwasaka, Ueno, & Curtis, 2000; Teodori et al., 2006), or from differential resistance experienced by current flowing with or against the magnetic field (Mondal, Fontanesi, Waldeck, & Naaman, 2015; Ron Naaman & Waldeck, 2015).

It occurred to us that under such circumstances, the polarised spin population may be detectable. Its spontaneous relaxation to equilibrium may take place by both thermal and radiative processes (Eaton, Eaton, Barr, & Weber, 2010; Goldfarb & Stoll, 2018). For a single fruit fly, an upper bound of the total energy released in the process of relaxation is given by the product of fully polarised electron current and free electron Zeeman energy in the applied magnetic field (115 μ eV/Tesla), say 100 pW for a 1 μ A current at 1T. Even if only a small fraction, say 10^{-4} , of this energy, were radiated in

¹ To whom correspondence should be addressed, lucaturin@me.com

response to an easily achievable magnetic field of .1 T, the emitted power would be of the order of a few femtowatts at 3-4 GHz. Our previous electron spin resonance spectroscopy (ESR) studies on electron spin in *Drosophila* (Turin & Skoulakis, 2018; Turin, Skoulakis, & Horsfield, 2014a) suggested fruit flies might be a good organism to look for emission, given their good transparency to radiofrequency even in the X-band, their ease of handling, their sensitivity to anesthetics and the powerful genetics tools available for their study. Commercial continuous-wave (CW) ESR spectrometers are ill-suited to study emission, however, because the incident RF beam can typically be turned down but not off, RF shielding is not optimal, and the cavity is tuned for maximum Q, which is undesirable for emission experiments where sample absorption must be kept low, not maximised. We therefore built two setups specifically designed to measure RF emission in fruit flies. Here, using this new instrumentation, we report the detection of nonthermal RF emitted from a living organism.

Methods The magnetic field in which the flies are immersed consists of two components: a fixed or slowly-varying field provided by a bench electromagnet (DSXG-100, Dexing Magnet) powered by a F-2030 power supply; and a modulation field provided by one or two solenoids (see below), fed from a sine wave generator via a 100W class-D audio amplifier (ST Microelectronics TDA7498) through a series resistor and capacitor to achieve the desired LC resonant frequency of ≈ 14 kHz. The sine wave signal serves as a reference for the lock-in amplifier. Following continuous-wave (CW) EPR practice, to study magnetic field dependence and improve the signal/noise ratio, we add a modulating magnetic field component to the slowly varying background field and measure the modulated emitted RF using lock-in detection. We are interested in detecting signals which vary in a resonant fashion with the magnetic field. In conventional CW ESR, this is achieved by lock-in detection at the magnetic field modulation frequency to obtain a differential signal proportional to the slope of the underlying absorption curve. Given the uncertainty about the signal phase in our experiments, we used R- Φ (modulus-phase) recording mode and only recorded modulus.

C-Band (4.5-4.8 GHz) waveguide setup. We enclosed *Drosophila melanogaster* wild type (W1118 strain) flies in a 4 mm ID PTFE tube situated at one end of a section of WR229 waveguide. To allow the WR229 waveguide to fit between the poles, the electromagnet pole pieces were ground from the original 30 mm separation to give a 36 mm pole gap and the end flange of the waveguide was trimmed along the short dimension to 34 mm to fit. The waveguide is terminated at the other end, approx 1 metre of waveguide away, by a C-band low-noise block (LNB, New Japan Radio model NJS8488U). The LNB mixes incoming RF at 4.5-4.8 GHz with the signal of a local oscillator at 5.76 GHz to produce a down-converted signal at 900-1200 MHz with 59-66 dB gain. That signal is fed to a logarithmic power detector (Minicircuits ZX47-60LN-S+) and on to an Ametek 7265 DSP Lock-in amplifier.

The modulating magnetic field is external to the waveguide and is provided by a solenoid made of 0.8 mm diameter copper wire (inductance 530 μ H) in series with a 490 nF capacitor. The coil is wound around a ferrite pot core to confine the magnetic field lines and avoid losses in the electromagnet pole pieces. The solenoid-pot core assembly is held on the end of a brass tube clamped in a micropositioner to allow precise three axis-movement. In order to avoid as far as is possible attenuation of the modulation field by eddy currents, the waveguide is terminated by a window consisting of a piece of aluminum foil glued to a 2mm-thick PTFE plate cut to the size of the flange. The ferrite core, while necessary, introduces some additional complications. First, it will concentrate field lines within itself

and dilute them elsewhere, so that the transverse DC field in front of the core will be lowered. The field inhomogeneity is relatively unimportant in our case because in experiments using a single fly the size of the specimen (2mm) is still small compared to the field gradient. Second, core inductance will decrease with increasing magnetic field as a result of gradual saturation of the ferrite, and therefore the resonant frequency of the LC circuit made up of the solenoid and series capacitor will fall. This is compensated by lowering the quality factor of the LC resonant circuit by adding 3.3Ω (100W rated) series resistance. Third, the magnetic field produced by the core at a given amplifier gain setting will vary with DC magnetic field. Insofar as peak positions rather than absolute amplitudes were of primary interest, this did not need addressing at this stage.

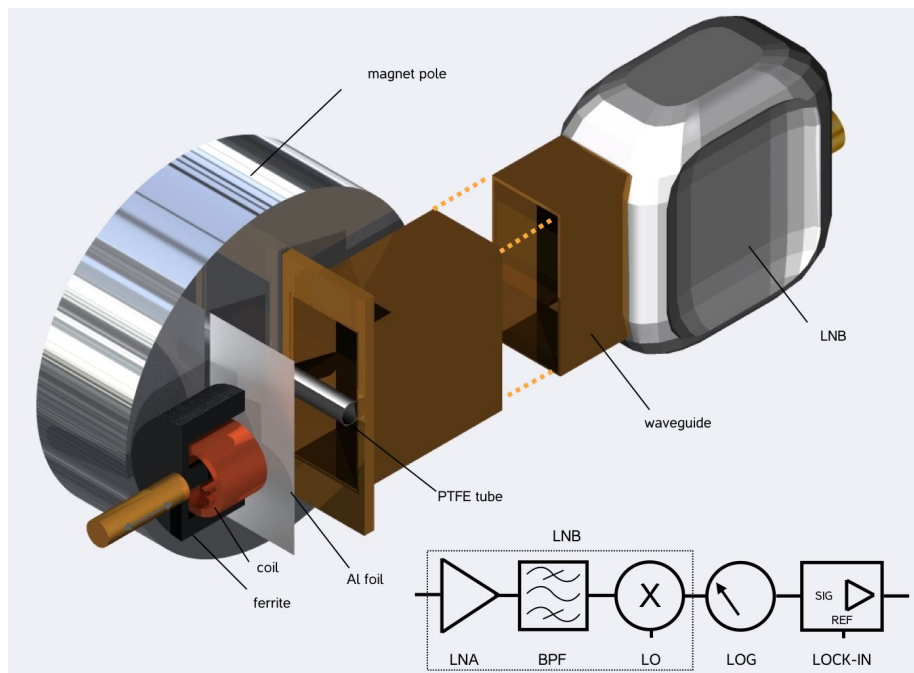


Figure 1: Exploded diagram of the waveguide experimental setup. Not shown: the PTFE backing of the aluminum foil, the mirror-image second pole piece of the electromagnet, and a thin sheet of plastic for electrical insulation between the waveguide and pole pieces to avoid current loops. The total WR-229 waveguide length is about 1 m and includes a 90-degree turn. The ferrite pot coil is mounted on a micropositioner for three-axis adjustment. Then signal chain (bottom right) consists of a low-noise amplification stage, a stripline bandpass filter, and a mixer with a local oscillator (LO), all within the LNB, followed by a logarithmic power meter (Minicircuits ZX47-60LN-S+) and an Ametek 7265 DSP lock-in amplifier.

The RMS noise measured on the power detector is approximately 50 mV at an average signal of -1.36 V corresponding to approximately -30 dBm power, with a gain slope of -25 mV/dB. The gain of the setup was calibrated by replacing the endplate with a WR229 flange-to-SMA adapter and feeding it with a fully AM-modulated RF signal (from a Windfreak Technologies SynthHD USB RF generator) attenuated to -120 dBm, to give an approximate power of 1 femtowatt. The main advantages of the waveguide setup are excellent RF quiet provided by the closed waveguide, ease of calibration, and separation between the heat produced in the modulation coil and the fly sample. Its main disadvantages are that the magnetic coupling of the flies to the waveguide is sensitive to distance from the endplate and exact position, as is the coupling of the flies to the modulation. When performing experiments, there is no independent way to make sure that both couplings are good and

measurements are therefore hit-and-miss. Another disadvantage is that it is not easy to extract the fly tube, and put it back in the exact same position, or to pass gases through it.

S-Band (2.6 GHz) resonator setup. We used a resonator of a re-entrant Φ -shaped design (Ciuffini & Sotgiu, 1983) built for these experiments by www.imagtech.it. It is tuned to approximately 2.6 GHz, and achieves high separation between electrical and magnetic coupling such that the central cavity (I) is uniformly coupled magnetically while being situated at an electric field minimum, one of the side arms (O) being used for coupling). A PTFE tube containing approximately 10 flies is inserted in the central tube. The coupling loop connected to an SMA snap-on plug in the coupling arm is set to overcoupling in order to maximize energy output from the cavity. The dimensions and dielectric properties of the cavity determine its tuning frequency, which in our case was in the range of 2.6 GHz, close to frequencies used by cell phones and WiFi.

Our intention was to avail ourselves of cheap accessory electronics in this frequency range, but in retrospect, this design choice turned out to have disadvantages. This is a busy part of the spectrum, and much ambient noise came from WiFi and cellphones. We found it necessary to encase the resonator in an earthed metallic box machined out of aluminum, incorporating holes for modulation current input to the two solenoids in a Helmholtz arrangement, an exit hole for a snap-on SMA signal connector from the coupling loop, and two flanged holes for air inlet and outlet to effect cooling.

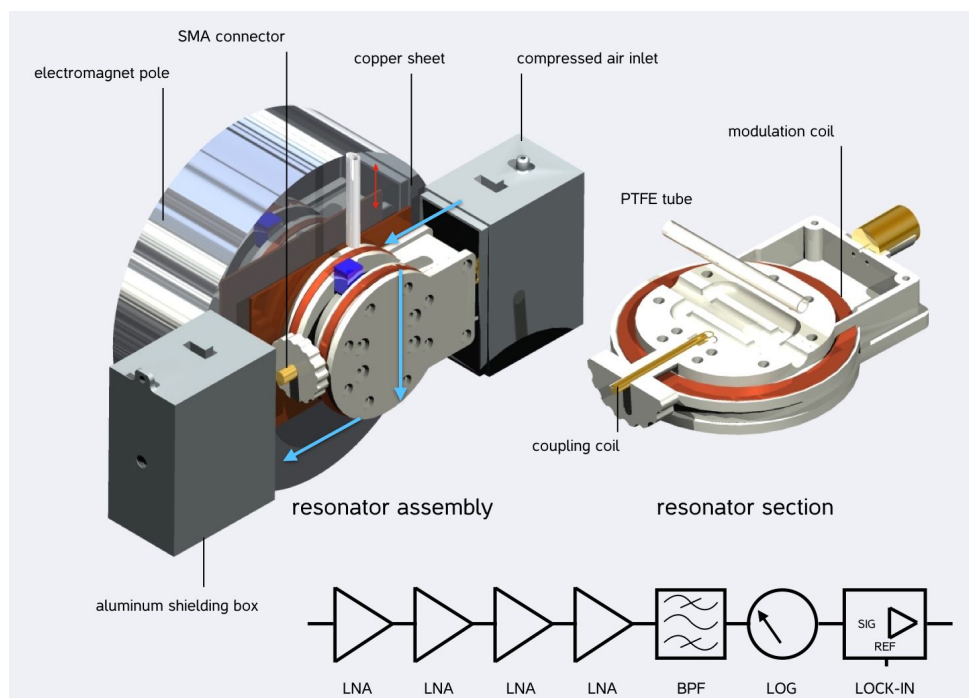


Figure 2: Left: Exploded diagram of the resonator experimental setup. Not shown: the mirror-image second pole piece of the electromagnet, and a second copper sheet for cooling. Air enters and exits the shielding box through symmetrically placed inlet and outlet (only inlet is visible). Airflow (blue arrows) within the box is constrained by plastic blocks indicated in dark blue to flow down the resonator tube and along both halves of the box before exiting from the bottom outlet. Right: the resonator sectioned down its middle, showing the shape of the resonant cavity, the position of the adjustable coupling coil in one of the arms and the connector to the modulation coils at the back. The signal processing chain is shown at bottom right it consists of four low-noise amplifiers (Minicircuits ZX60-P103LN+) in series, a 2.45-2.7 GHz band-pass filter (Microdyne), a logarithmic power meter (Minicircuits ZX47-60LN-S+) and an Ametek 7265 DSP Lock-in amplifier.

An advantage of this setup are that the design of the resonator ensures that the flies are optimally coupled whatever their position inside the resonator. A disadvantage is that the need for holes in the shielding box necessarily allows some RF noise in. Another disadvantage is that the heat from the modulation coils must be dissipated to make sure the flies are kept at a temperature lower than 28-29C. To this end two copper sheets .5 mm in thickness were glued to the side of the resonator and thermally connected to the metal retaining screws with thermal paste. In addition, two small wedges of sponge were positioned in the resonator grooves in such a way as to ensure that air circulated down the central tube, both around and within the PTFE tube containing the flies. To this end, the flies were constrained in the middle two-thirds of the tube by small PTFE plugs triangular in shape to allow air flow without letting flies escape. For exposure to chloroform, the fly tube was removed from the resonator, exposed to chloroform vapor for a few seconds and replaced in the tube.

Results.

General remarks: Signals are *not always present* in every batch of live flies. In the waveguide experiments, If the endplate was properly adjusted onto the waveguide flange, excellent radio quiet was obtained, monitored on an oscilloscope displaying the output of the logarithmic power meter, and there were no visible artifacts from outside sources. We are therefore confident that when a signal is seen in the waveguide setup, it emanates from what is inside the waveguide. We attribute the hit-and-miss in part to the difficulty in positioning exactly the PTFE tube and the external coil with respect to each other and to the endplate to obtain both maximum modulation field and maximum magnetic coupling to the waveguide endplate. Indeed, once a signal was present, small movements of the micropositioner holding the modulation coil outside the waveguide caused large amplitude variations in it.

This said, that cannot be the only reason for the absence of signal in many resonator experiments (see below), in which exact position should not matter. There is clearly an additional, currently unidentified, source of variability. This report is therefore a work in progress. We believe the RF emission observed in resonator experiments, when present, is a genuine signal for the following reasons: **1-** Long-term control recordings of the resonator lasting up to 48 hours (figure 6) show no events resembling the signal. **2-** The dependence of the signal on magnetic field exhibits resonant peaks (figures 3,4 and 5). It is hard to see what artifact could be resonant with a slowly-varying magnetic field **3-** The signal is only detected when modulation is on (figure 7A) **4-** The signal only occurs when the flies are alive and disappears gradually as they die (figure 7B) **5-**The signal disappears in flies exposed to chloroform vapor (figures 4 and 5), and **6-** We have now observed the emitted RF behaving similarly in three different setups, the first one using permanent magnets for steady field and lower modulation frequencies (USPTO Patent No. 20180126010, 2018), as well as the two electromagnet setups described in this report.

Waveguide experiments at 4.5-4.8 GHz. Figure 3 shows the best trace obtained to date with the waveguide setup. The exceptionally quiet RF environment, high gain and low noise figure of the LNB-waveguide arrangement afford an excellent signal/noise ratio. The trace obtained a few minutes earlier with an empty tube (black and inset) shows gaussian noise filtered by the output time constant of the lock-in amplifier (1 second). The red trace with live flies shows several clear resonant peaks. Despite the unquestioned advantages in radio quiet and signal/noise ratio, we felt that the lack of

reliable relative positioning of the solenoid, end-plate and flies added an unnecessary difficulty to the experiments, and we focused on the resonator setup.

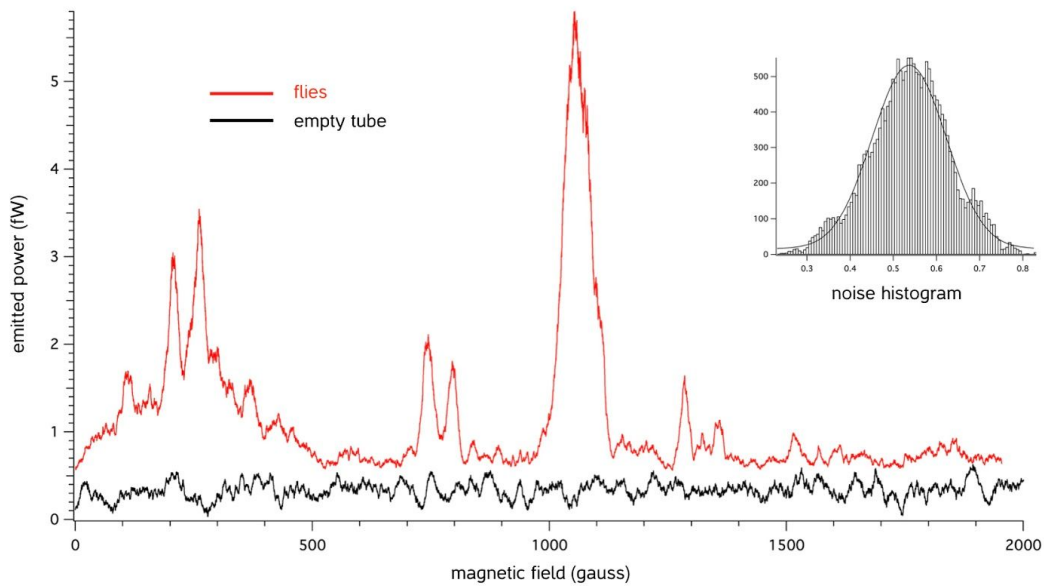


Figure 3: Radiofrequency emission from ≈ 10 fruit flies contained in a Teflon tube positioned at the end of a WR229 waveguide, detected at 4.5–4.8 GHz with a room temperature C-band satellite receiver. The value of the steady magnetic field is given in the abscissa, emitted RF power in the ordinate. The signal is detected using a logarithmic power meter and a lock-in amplifier, with a modulation frequency of 16 kHz, a width of ≈ 90 gauss and a response time constant of 1 second (6dB per octave). The steady magnetic field is ramped at approximately 10 gauss/second. The trace is exponentiated to restore linearity. It clearly shows several resonant features at 200, 270, 770, 800, 1050 and 1300 gauss. The red trace shows the signal when live flies are present in the tube. The black trace is taken a few minutes earlier with no flies in the tube and has the properties of gaussian noise (see inset histogram of black trace). The empty tube trace has been shifted downwards in the main graph by 0.2 fW for clarity.

Resonator experiments at 2.6 Ghz

Slow recordings. The resonator setup has the advantage of a high degree of magnetic coupling to the fly at the expense of greater RF interference because it does not in itself provide a Faraday cage. Our initial design criteria planned for interfacing with generators and circulators, to eventually build a full ESR setup. 2.6 GHz was chosen to ensure that such components were available and affordable, insofar as they are mass-produced for cellular and WiFi use. This turned out to create its own difficulties, because that RF band is busy, and the low-noise measurements demanded by our experiments required close attention to additional shielding. We therefore designed a tight-fitting Faraday “box” in two parts with a lip overlap. Bored holes at each end to allow connection of the modulation and the amplifier chain. This greatly reduced noise, and in practice allowed measurements to be made with a lock-in output filter time constant of 10 seconds, 6dB/octave. Modulation frequency was set to 13.9 kHz, the resonant frequency of the 376 μH solenoid coils in series with 455 nF. Resonance was determined by using an external pickup coil made of a few turns of copper wire and setting frequency manually to the (rather shallow) maximum magnetic field value. The modulation coils give 20 gauss/A, and large values of modulation were found to be necessary to detect the signal,

a fact which may be important in interpreting the results (see discussion). Conventional Class D and class AB audio amplifiers struggled with these frequency and current levels and sometimes gave parasitic oscillations leading to excess heating in the solenoid. We eventually settled on an inexpensive class D amplifier capable of a maximum output of 7A at 14 kHz without overheating or damage. In the experiments described below the maximum modulation of 140 gauss was used.

An accidental discovery increased the chance of observing a signal: while we were dealing with airflow within the box to keep the temperature within limits tolerable by the flies, we noticed that a brief period of nonlethal heat stress around 30C caused the flies to emit signal more reliably. We did this deliberately in a number of experiments. Figure 4 illustrates one such experiment. The black trace (shifted downwards by .1 units for clarity) was taken with an empty tube. The first trace with flies, slightly above normal temperature is shown in blue and a small signal is visible around 750 and 850 gauss. The second trace 181 minutes later is shown in red and a large signal is clearly visible around 800 gauss. Note that practically the entire red trace is above background, and that smaller signals can be seen both below and above the main peak. After exposure to chloroform, the signal returns to baseline (green trace, also shifted downwards by .1 units for clarity).

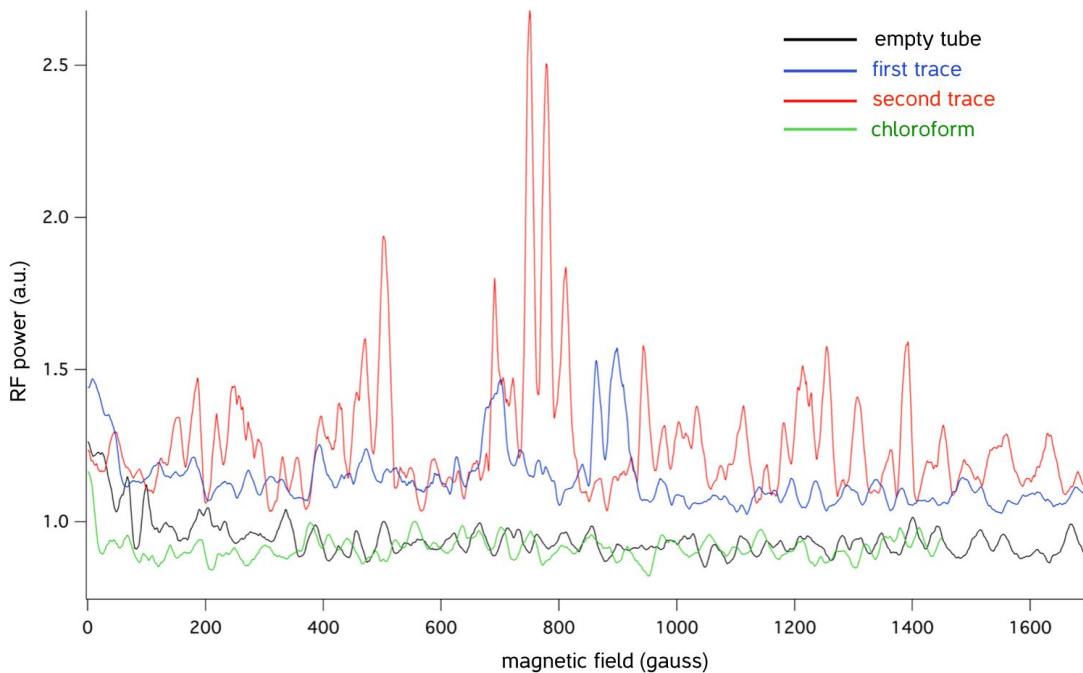


Figure 4: Four traces from a heat-stress experiment in the 2.6 GHz resonator. The bottom two traces have been shifted downwards for clarity. See text for details. The sweep from 0 to 2000 gauss took 30 minutes, and the lock-in output time constant was 10 seconds, 6dB/octave. The ≈ 18000 point traces were smoothed with a 100-point box filter after acquisition for noise reduction. The ordinate is in arbitrary units because calibration of the resonator setup is difficult insofar as the degree of coupling between cavity and pick-up coil is unknown. See figure 3 for a better measurement of likely power output.

A similar but larger signal is shown in figure 5. Conditions are the same as in figure 4, i.e. 30-minute sweep and 10-second output time constant. The flies were subjected to a brief heat stress of 5 minutes. Most of the signal occurs between 650 and 1200 gauss. Fluctuations in the peak are larger than before and after, suggesting that the peak may have some substructure unresolved under the current measuring conditions. A brief exposure to chloroform 35 minutes later abolishes the signal (black trace).

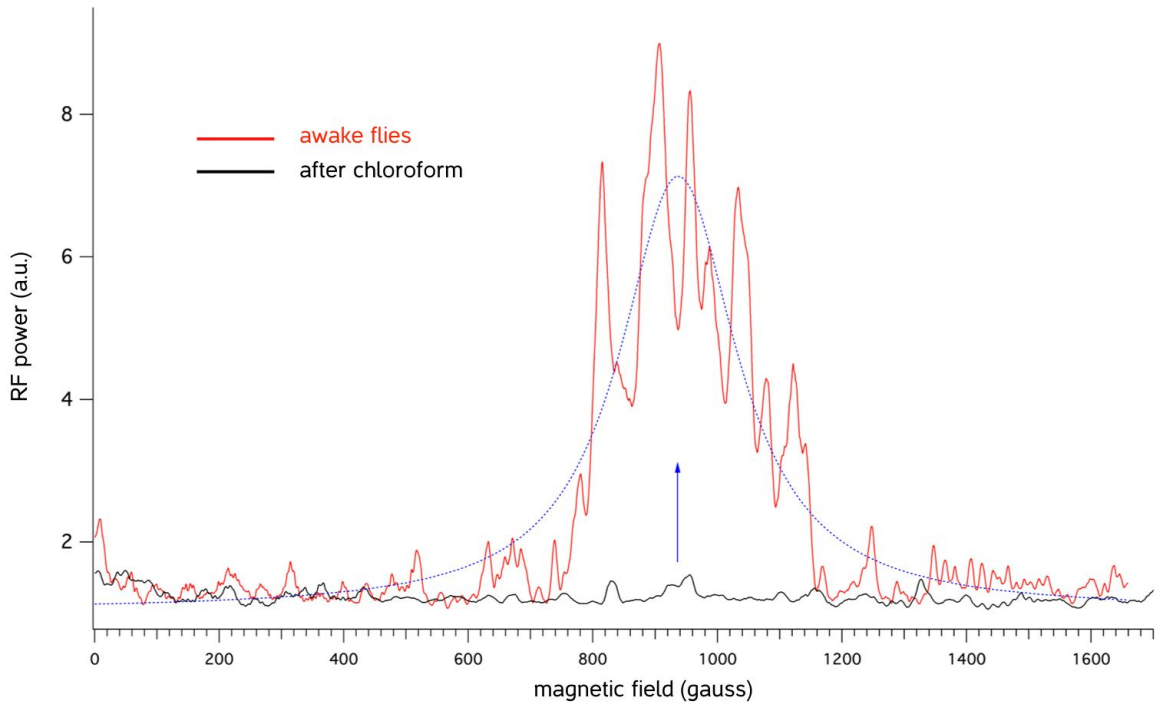


Figure 5: The best trace obtained to date in the 2.6 GHz resonator. See text for details. The sweep from 0 to 2000 gauss took 30 minutes, and the lock-in output time constant was 10 seconds, 6dB/octave. The ≈ 18000 point traces were smoothed with a 100-point box filter after acquisition for noise reduction. The ordinate is in arbitrary units because calibration of the resonator setup is difficult insofar as the degree of coupling between cavity and pick-up coil is unknown. The dotted blue line is a Lorentzian fit with a midpoint of 930 gauss (arrow).

Naturally, the question arises of whether the signals shown in figures 4 and 5 are merely random glitches of exceptional magnitude that happen to take place during a sweep. The radiofrequency environment is very variable, and occasional large pulses are seen in the log detector trace, so this possibility cannot be excluded *a priori*. To test for this we made long-term recordings of the signal under the same conditions as figures 4 and 5 with an empty tube and modulation on over a period of 17.8 hours. The complete trace is shown in Figure 6A. No transients above noise are visible. We are therefore confident that the signal in figure 5 is not due to a random external perturbation.

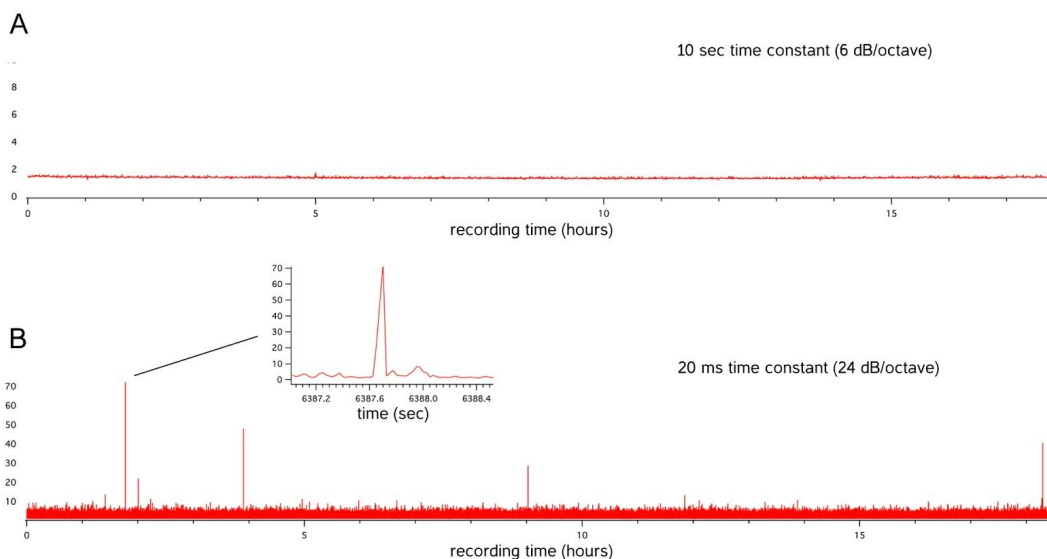


Figure 6: A: Continuous 17.8 hours recording of lock-in signal output with empty resonator under the same conditions and at the same scale as the experiment depicted in **figure 5** (red trace). The trace shows no activity at all, and the noise level is identical to that observed in chloroform in figure 5 (black trace). **B:** Continuous 18.4 hours recording of lock-in signal output with empty resonator under the experimental conditions used for **figure 7A**, with modulation on. 8 glitches above noise are visible in the trace, i.e. approximately one every 140 minutes. All of them behave as the largest one does (inset), i.e. last ≈ 100 ms. The rest of the trace is baseline noise. Over 18.4 hours, the signal integrates to $2 \cdot 10^4$, as compared to $3.68 \cdot 10^5$ in 3 minutes for the experiment depicted in 7A, red trace.

Fast recordings. A further improvement in background noise was obtained by wrapping the resonator Faraday box in a bag made of two layers of conductive RF fleece (Aaronia 100-dB X-dream) for additional shielding. The fleece is sufficiently porous that the air outlet is unimpeded. Cable and tube exits from the fleece bag were secured with ring ties. Figure 6B shows the noise trace obtained over 18.4 hours with this method using a much shorter (20ms) lock in time constant.

This shortening of the lock-in output time-constant from 10 seconds to 20 ms (24 dB/octave filter) allowed us to measure the signal with higher bandwidth. Previous experiments (USPTO Patent No. 20180126010, 2018) using permanent magnets for the steady magnetic field had provided hints that the signal came in short pulses lasting a fraction of a second. Such pulses would be smoothed into a noisy continuous trace under the recording conditions of figures 3, 4 and 5, but could possibly be resolved with a shorter time constant. Figure 7A shows two successive 3-minute magnetic field sweeps taken on the same set of flies, first without (black), and then with modulation (red trace). The black trace is indistinguishable from gaussian noise. A striking increase in the number of short RF pulses is seen when the modulation is turned on. Compare with the long-term trace taken with modulation but without flies shown in figure 6B under the same measurement conditions.

In order to assess the pulsed signal more quantitatively, the trace was integrated after setting the zero to the median of the trace obtained without modulation, such that gaussian noise alone would integrate to zero. The integrated traces are shown in figure 7B. The red and black traces correspond to the traces in figure 7A, the orange trace is taken 8 minutes later with the modulation on, the yellow one 5 minutes later. The flies are thermally stressed, and the signal is decreasing. The next traces (orange and yellow) give a decreasing signal, and finally one indistinguishable from baseline (not shown). Upon opening the resonator, the flies are found to have died. The power spectra of the signals with and without modulation show an approximately 100-fold difference in signal power at low frequencies, gradually decreasing as frequency rises, but remaining detectable all the way to the Nyquist frequency of these measurements, 2.5 kHz.

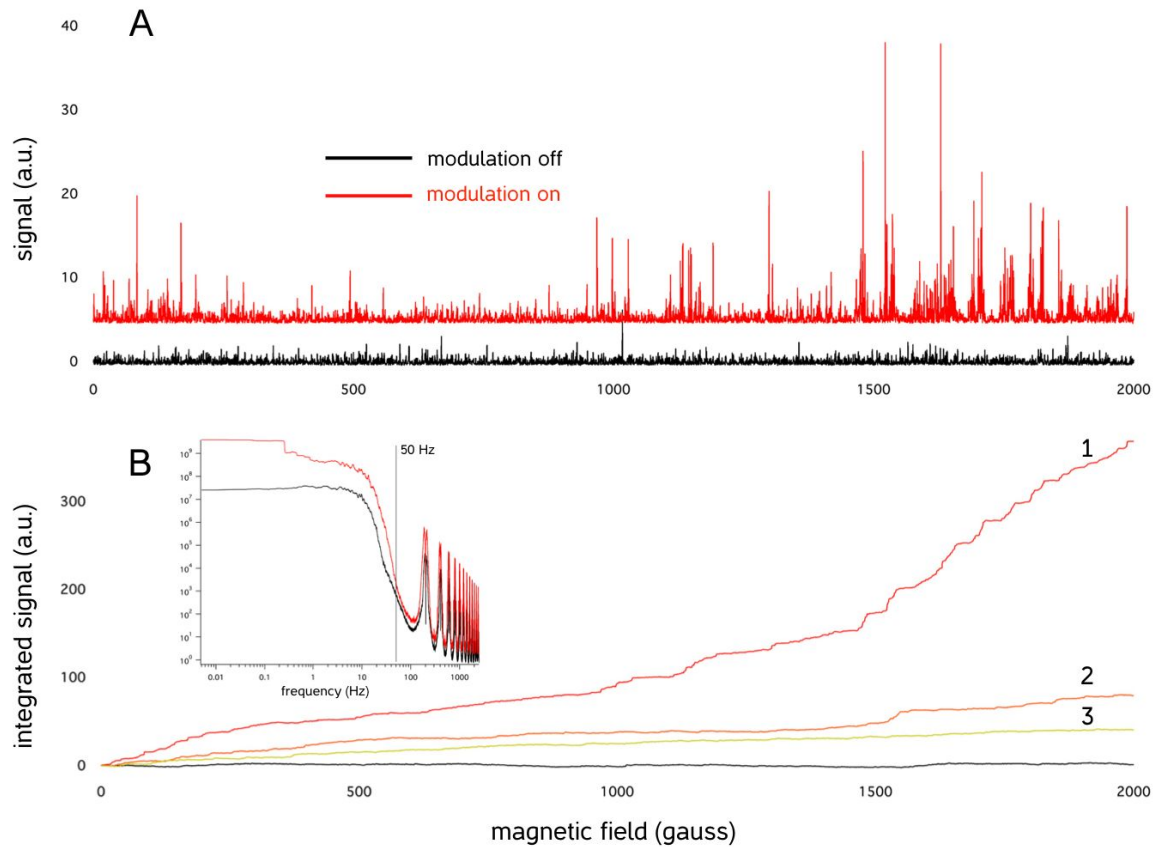


Figure 7: **A:** Two 3-minute magnetic field sweeps recorded with a 20 ms lock-in output time constant. In black, first sweep without modulation. In red, immediately following, with 140 gauss modulation (and therefore heating) switched on. Sampling frequency 5 kHz, 16 bits resolution. A marked increase in pulse-like signals is seen when the modulation signal is on. The red trace has been shifted up by 5 units for clarity. **B:** the traces in A integrated from $T=0$ to 180 seconds. Trace 2 (orange) is taken 8 minutes after the red one and shows the signal decreasing in amplitude, trace 3 (yellow) 5 minutes later. **Inset:** power spectra of the two traces in A. The power spectrum (magnitude squared) is dominated by the output filter time constant, but the signal power with modulation on is two orders of magnitude larger at low frequencies and remains above the no-modulation spectrum at all frequencies up to and beyond the nominal cutoff frequency of 50 Hz, including in the stopband ripples above 100 Hz. This suggests that the signal added by modulation has a wider bandwidth than current measurements allow.

Discussion. Many experimental aspects of the signals we report remain unsettled and require further study. First, the factor governing the overall presence or absence of signal remains to be determined. Our temperature experiments suggest that it may be related to a stress response, or possibly to an increase in metabolism or activity due to the rise in temperature. Second, the relationship of signal amplitude to modulation amplitude is unclear at the present time. It is our impression that the signal depends nonlinearly on modulation amplitude and that a threshold may exist for RF generation. If indeed this is spontaneous emission, its rate should go up as the third power of magnetic field (Henderson & Imbusch, 1989), and the derivative signal we measure should increase with the square of the modulation field. Third, the origin of the RF pulses is unknown. We recall that the tube contains several flies. Are they all emitting? Single-fly experiments will be needed to address this question. Fourth, the possibility of stimulated emission (Oxborrow, Breeze, & Alford, 2012) within the resonator cavity, accounting for the nonlinearity and intermittency of the responses cannot yet be

ruled out. It should also be recalled that we are measuring signals from a few flies weighing a milligram each. Signals from larger organisms, if they scale linearly with mass, should be much larger and should justify the effort to scale up the experiments to, say, a mouse-sized device or larger.

Radiofrequency emissions from living systems have been previously reported (Cazzamalli, 1960; Kazhinskiy, 1962, 1963). For a comprehensive review of Soviet work see (Kernbach, 2013). Magnetic field was not used as a controlling variable in any of these studies. The lack of recent interest is no doubt in part due to the poorly controlled experimental conditions and emphasis on biological radiocommunication of many of these early reports. Emission of radiofrequency does not in any way guarantee its reception, and the present study makes no claims as to the use of RF as a means of communication. We are instead interested in the mechanism by which the signals are generated, and in what they tell us about cellular processes. Radiofrequency emissions from chemical reactions are well understood, but they arise from polarisation of nuclear spins (Buchachenko & Frankevich, 1993; Hore, Joslin, & McLauchlan, 1979) and therefore occur at NMR frequencies, one or two orders of magnitude lower.

Our motivation for measuring RF emission in this frequency range and in a magnetic field was the finding, proposed by Naaman and colleagues (Naaman & Waldeck, 2012) that electron currents flowing through chiral media become spin polarised in the direction of travel. *In vitro* experiments have confirmed this in a variety of systems, but the mechanism (chirally induced spin-selectivity or CISS) by which it occurs is still debated (Hedegard & Dalum, 2019). Regardless of theory, if experimentally confirmed *in vivo* by RF emission, the generation of spin-polarised electron currents would bring biological electronics into the realm of spintronics. This would have consequences for biological electrochemistry (Mondal, Fontanesi, Waldeck, & Naaman, 2016). It would also affect the interpretation of biological ESR spectra, since absorption of microwaves by unpaired electrons crucially depends on their thermal equilibrium distribution (Poole, 1967).

While our results make a case for the existence of emitted RF, its relationship to CISS remains unclear. On the one hand, a clear dependence on magnetic field is seen, which, together with the RF frequency, is a strong indication that a magnetic species out of thermal equilibrium, with a gyromagnetic ratio close to that of the electron, is responsible for the RF emission. On the other hand, at least in the simplest interpretation of the phenomenon as the reverse of absorption, emission does not occur solely in well-defined regions of the background magnetic field. Some of our resonator data (see figure 5) is consistent with emissions from a species with a Landé g-factor close to 2 (≈ 930 gauss at 2.6 GHz), but there also appear to be emissions at lower and higher field values. The main peak in figure 3, for example, even accounting for magnetic field distortion by the ferrite core, does not match the expected value of ≈ 1600 gauss expected for free electrons at 4.5 GHz. Lower values may be due to higher g-factors, commonly seen in biology, for example when metal ions are involved. Higher magnetic field values than those corresponding to $g=2$ require a different explanation.

A striking feature of the results reported here is that the RF power emitted by the fruit flies is not the result of energy input into the system: it is instead powered by the flies' own metabolism. If CISS is responsible, the magnetic field in which the flies are immersed merely diverts a small part of the electrochemical force driving polarised electron currents into RF emission. Assuming a total oxidative metabolism energy of 1.4 eV, emission at 4GHz would represent an energy loss to RF photons of 15 μeV , i.e. approximately 10 parts per million. The RF emission we observe can be viewed as a passive,

non-invasive measurement of the underlying electron currents, whose functional importance remains to be determined. Its ultimate interest and usefulness will depend on identifying the currents' origin and function in the living organism.

The fact that the RF emission varies rapidly is also remarkable. Most electron currents in living systems flow through mitochondria, and some or all of the RF emission may be thus related to mitochondrial metabolism. A constant RF emission, would be expected for example from a steady mitochondrial current flowing to oxygen. A rapidly varying current indicates instead that something more complex is going on. This could conceivably be due to mitochondrial electron currents switching on and off. However, the fact that the signals disappear in chloroform, whereas respiration is only mildly inhibited (Turin & Skoulakis, 2018), suggests instead a direct connection with the central nervous system. Note that these two possibilities are not mutually exclusive: there is much evidence connecting the still mysterious action of general anesthetics to mitochondrial function (Eckenhoff & Johansson, 1997; Hoppel, Sedensky - : The Journal of ..., & 2002, 2002; Morgan, Sedensky - The Journal of, & 1999, 1999; Woll, Dailey, & Eckenhoff, 2018). Our previous work on olfaction has established a connection between electron currents, odorant sensing and G-protein activation more generally (Franco, Turin, Mershin, & Skoulakis, 2011; Gane et al., 2013; Gehrckens, Horsfield, Skoulakis, & Turin, 2019; Horsfield, Haase, & Turin, 2017; L. Turin, 1996), while that on general anesthesia has shown a correlation between spin content of *Drosophila* (as measured by CW ESR) and general anesthetic action (L. Turin & Skoulakis, 2018; Luca Turin, Skoulakis, & Horsfield, 2014b).

The RF emissions described in this report may therefore reflect neuronal activity. If they are related to cellular respiration and imaging can be achieved, they may provide a new technology to measure oxygen consumption. If instead the RF signals are correlated with high-speed neuronal activity, then a new window may be opened into neuronal physiology. Finally, if they vary in a reproducible fashion according to brain state, they may enable diagnostics and device control via RF.

Contributions. AG and LT designed and performed the experiments. AS designed the resonator and its amplification chain. LT wrote the paper, AG and AS reviewed the paper.

Acknowledgments. We thank Makis Skoulakis, Andrew Horsfield, Ron Naaman and Yossi Paltiel for discussions and encouragement. We are very grateful to Peter Hore and Aharon Blank for advice on theory and experimental method. This project was funded by DARPA Biological Technologies Office (grant N65236-18-1-1000 to LT) and we thank them for their generous support. LT thanks the Stavros Niarchos Foundation for support.

Buchachenko, A. L., & Frankevich, E. L. (1993). *Chemical Generation and Reception of Radio-and Microwaves*. John Wiley & Sons.

Cazzamalli, F. (1960). *Il Cervello Radiante*. Milan: Ceschina.

Ciuffini, V., & Sotgiu, A. (1983). Lumped parameters for re-entrant resonators. *Journal of Physics D: Applied Physics*. Retrieved from <https://iopscience.iop.org/article/10.1088/0022-3727/16/11/011/meta>

Eaton, G. R., Eaton, S. S., Barr, D. P., & Weber, R. T. (2010). *Quantitative EPR*. Springer Science & Business Media.

Eckenhoff, R. G., & Johansson, J. S. (1997). Molecular interactions between inhaled anesthetics and proteins. *Pharmacological Reviews*, 49 (4), 343–367.

Franco, M. I., Turin, L., Mershin, A., & Skoulakis, E. M. C. (2011). Molecular vibration-sensing component in *Drosophila melanogaster* olfaction. *Proceedings of the National Academy of Sciences*, 108 (9), 3797–3802.

- Gane, S., Georganakis, D., Maniati, K., Vamvakias, M., Ragoussis, N., Skoulakis, E. M. C., & Turin, L. (2013). Molecular vibration-sensing component in human olfaction. *PLoS One*, 8 (1), e55780.
- Gehrckens, A. S., Horsfield, A. P., Skoulakis, E., & Turin, L. (2019). Gated electron transport in rhodopsin and its relevance to GPCR activation (p. 650531). <https://doi.org/10.1101/650531>
- Goldfarb, D., & Stoll, S. (2018). *EPR Spectroscopy: Fundamentals and Methods*. John Wiley & Sons.
- Gutierrez, R., Díaz, E., Naaman, R., & Cuniberti, G. (2012). Spin-selective transport through helical molecular systems. *Physical Review B, Condensed Matter*, 85 (8), 081404.
- Hedegard, P., & Dalum, S. (2019). Theory of Chiral Induced Spin Selectivity. *Nano Letters*. <https://doi.org/10.1021/acs.nanolett.9b01707>
- Henderson, B., & Imbusch, G. F. (1989). *Optical properties of inorganic solids*. Oxford: Oxford University Press.
- Hoppel, C. L., Sedensky - : The Journal of ..., M. M., & 2002. (2002). Mitochondrial defects and anesthetic sensitivity. *Anesthesiology.pubs.asahq.org*. Retrieved from <http://anesthesiology.pubs.asahq.org/article.aspx?articleid=1945081>
- Hore, P. J., Joslin, C. G., & McLauchlan, K. A. (1979). The role of chemically-induced dynamic electron polarization (CIDEP) in chemistry. *Chemical Society Reviews*, 8 (1), 29–61.
- Horsfield, A. P., Haase, A., & Turin, L. (2017). Molecular recognition in olfaction. *Advances in Physics: X*, 2 (3), 937–977.
- Hunter, A. S. (1964). Effects of temperature on *Drosophila*—I. respiration of *D. melanogaster* grown at different temperatures. *Comparative Biochemistry and Physiology*, 11 (4), 411–417.
- Iwasaka, M., Miyakoshi, J., & Ueno, S. (2003). Magnetic field effects on assembly pattern of smooth muscle cells. *In Vitro Cellular & Developmental Biology. Animal*, 39 (3-4), 120–123.
- Kazhinskiy, B. B. (1962). *Biologicheskaya Radiosvyaz'*. Kiev, Ukraine: Izdatel'stvo Akademiy Nauk Ukrainskoy SSR.
- Kazhinskiy, B. B. (1963). *Biological Radio Communications*. Retrieved from <https://apps.dtic.mil/dtic/tr/fulltext/u2/415676.pdf>
- Kernbach, S. (2013). Unconventional research in USSR and Russia: short overview. Retrieved from <http://arxiv.org/abs/1312.1148>
- Kotani, H., Iwasaka, M., Ueno, S., & Curtis, A. (2000). Magnetic orientation of collagen and bone mixture. *Journal of Applied Physics*, 87 (9), 6191–6193.
- Mondal, P. C., Fontanesi, C., Waldeck, D. H., & Naaman, R. (2015). Field and chirality effects on electrochemical charge transfer rates: spin dependent electrochemistry. *ACS Nano*, 9 (3), 3377–3384.
- Mondal, P. C., Fontanesi, C., Waldeck, D. H., & Naaman, R. (2016). Spin-Dependent Transport through Chiral Molecules Studied by Spin-Dependent Electrochemistry. *Accounts of Chemical Research*, 49 (11), 2560–2568.
- Morgan, P. G., Sedensky - The Journal of, M. M., & 1999. (1999). GAS-1 A Mitochondrial Protein Controls Sensitivity to Volatile Anesthetics in the Nematode *Caenorhabditis elegans*. *Anesthesiology.pubs.asahq.org*. Retrieved from <http://anesthesiology.pubs.asahq.org/pdfaccess.ashx?url=/data/journals/jasa/931257/0000542-199902000-00031.pdf>
- Naaman, R., Paltiel, Y., & Waldeck, D. H. (2018). Chirality and Spin: A Different Perspective on Enantioselective Interactions. *Chimia*, 72 (6), 394–398.
- Naaman, R., & Waldeck, D. H. (2012). Chiral-Induced Spin Selectivity Effect. *Journal of Physical Chemistry Letters*, 3 (16), 2178–2187.
- Naaman, R., & Waldeck, D. H. (2015). Spintronics and chirality: spin selectivity in electron transport through chiral molecules. *Annual Review of Physical Chemistry*, 66, 263–281.
- Oxborrow, M., Breeze, J. D., & Alford, N. M. (2012). Room-temperature solid-state maser. *Nature*, 488 (7411), 353–356.
- Poole, C. P. (1967). *Electron Spin Resonance: A Comprehensive Treatise on Experimental Techniques*.
- Rees, D. (1983). Biopower. *Journal of Chemical Education*, 60 (4), 289.
- Teodori, L., Albertini, M. C., Uguccioni, F., Falcieri, E., Rocchi, M. B. L., Battistelli, M., ... Accorsi, A. (2006). Static magnetic fields affect cell size, shape, orientation, and membrane surface of human glioblastoma cells, as demonstrated by electron, optic, and atomic force microscopy. *Cytometry*, 69A (2), 75–85.
- Turin, L. (1996). A spectroscopic mechanism for primary olfactory reception. *Chemical Senses*, 21 (6), 773–791.
- Turin, L. (2018). *USPTO Patent No. 20180126010*. Retrieved from <http://www.freepatentsonline.com/y2018/0126010.html>
- Turin, L., & Skoulakis, E. M. C. (2018). Electron Spin Resonance (EPR) in *Drosophila* and General Anesthesia.

- In *Methods in enzymology* (Vol. 603, pp. 115–128). Academic Press.
- Turin, L., & Skoulakis, E. M. C. (2018). Electron Spin Resonance (EPR) in *Drosophila* and General Anesthesia. In Dmochowski, Ivan J. and Eckenhoff, Roderic G. (Ed.), *Methods in Enzymology (series)*. Elsevier.
- Turin, L., Skoulakis, E. M. C., & Horsfield, A. P. (2014a). Electron spin changes during general anesthesia in *Drosophila*. *Proceedings of the National Academy of Sciences*, *111* (34), E3524–E3533.
- Turin, L., Skoulakis, E. M. C., & Horsfield, A. P. (2014b). Electron spin changes during general anesthesia in *Drosophila*. *Proceedings of the National Academy of Sciences of the United States of America*, *111* (34), E3524–E3533.
- Varade, V., Markus, T., Vankayala, K., Friedman, N., Sheves, M., Waldeck, D. H., & Naaman, R. (2018). Bacteriorhodopsin based non-magnetic spin filters for biomolecular spintronics. *Physical Chemistry Chemical Physics: PCCP*, *20* (2), 1091–1097.
- Woll, K. A., Dailey, W. P., & Eckenhoff, R. G. (2018). Identification of General Anesthetic Target Protein-Binding Sites by Photoaffinity Labeling and Mass Spectrometry. *Methods in Enzymology*, *602*, 231–246.
- Zwang, T. J., Hürlimann, S., Hill, M. G., & Barton, J. K. (2016). Helix-Dependent Spin Filtering through the DNA Duplex. *Journal of the American Chemical Society*, *138* (48), 15551–15554.